A novel BN/TiO2/HNT nanocomposite for photocatalytic applications fabricated by electrospinning

Mahmoud Abid, Syreina Sayegh, Fida Tanos, Habib Belaid, Igor Iatsunskyi, Emerson Coy, Marc Cretin, Geoffroy Lesage, Abdesslem Ben Haj Amara, Mikhael Bechelany

A novel BN/TiO_2/HNT nanocomposite for photocatalytic applications fabricated by electrospinning

Mahmoud ABID [a,b], Syreina SAYEGH [a], Fida TANOS [a], Habib BELAID [a], Igor IATSUNSKYI [c], Emerson COY [c], Marc CRETIN [a], Geoffroy LESAGE [a], Abdesslem BEN HAJ AMARA [b,1] and Mikhael BECHELANY [a,*,1]

[a] Institut Européen des Membranes, IEM, UMR 5635, Univ Montpellier, ENSCM, CNRS, 34730 Montpellier, France

[b] Laboratory of Resources, Materials & Ecosystem (RME), University of Carthage, Faculty of Sciences of Bizerte, Zarzouna 7021, Tunisia

[c] NanoBioMedical Centre, Adam Mickiewicz University, Wszechnicy Piastowskiej 3, 61-614 Poznan, Poland

[*]Corresponding author
E-mail address: mikhael.bechelany@umontpellier.fr (M. Bechelany)
[1] Co-last authors

Abstract

Here, we fabricated non-toxic composite nanofibers by including controlled amounts of boron nitride (BN) nanosheets (5%), titanium oxide (TiO_2) nanofibers and halloysite nanotubes (HNT) with the aim of obtaining a good catalyst for acetaminophen (ACT) degradation. After annealing at 400 °C under air, we characterized the samples' morphological, structural, and optical features by scanning and transmission electron microscopy, Brunauer-Emmet-Teller analysis, X-ray diffraction, X-ray photoelectron spectroscopy, Fourier transform infrared spectroscopy and Raman spectroscopy. Under visible light, BN/TiO_2/HNT nanocomposite (5% of BN nanosheets and 5% of TiO_2) degraded more than 98% of acetaminophen after 3 hours. Moreover, the BN/TiO_2/HNT nanocomposite could be used for five cycles without significant changes in acetaminophen degradation rate. The acute toxicity and scavenging tests to monitor the formation of by-products and reactive species showed that $OH^{\bullet -}$, $O_2^{\bullet -}$, and h^+ played a major role in acetaminophen degradation. These results indicate that BN/TiO_2/HNT composite nanofibers can be used for photodegradation and open new prospects for developing tunable photocatalysts.

Graphical abstract

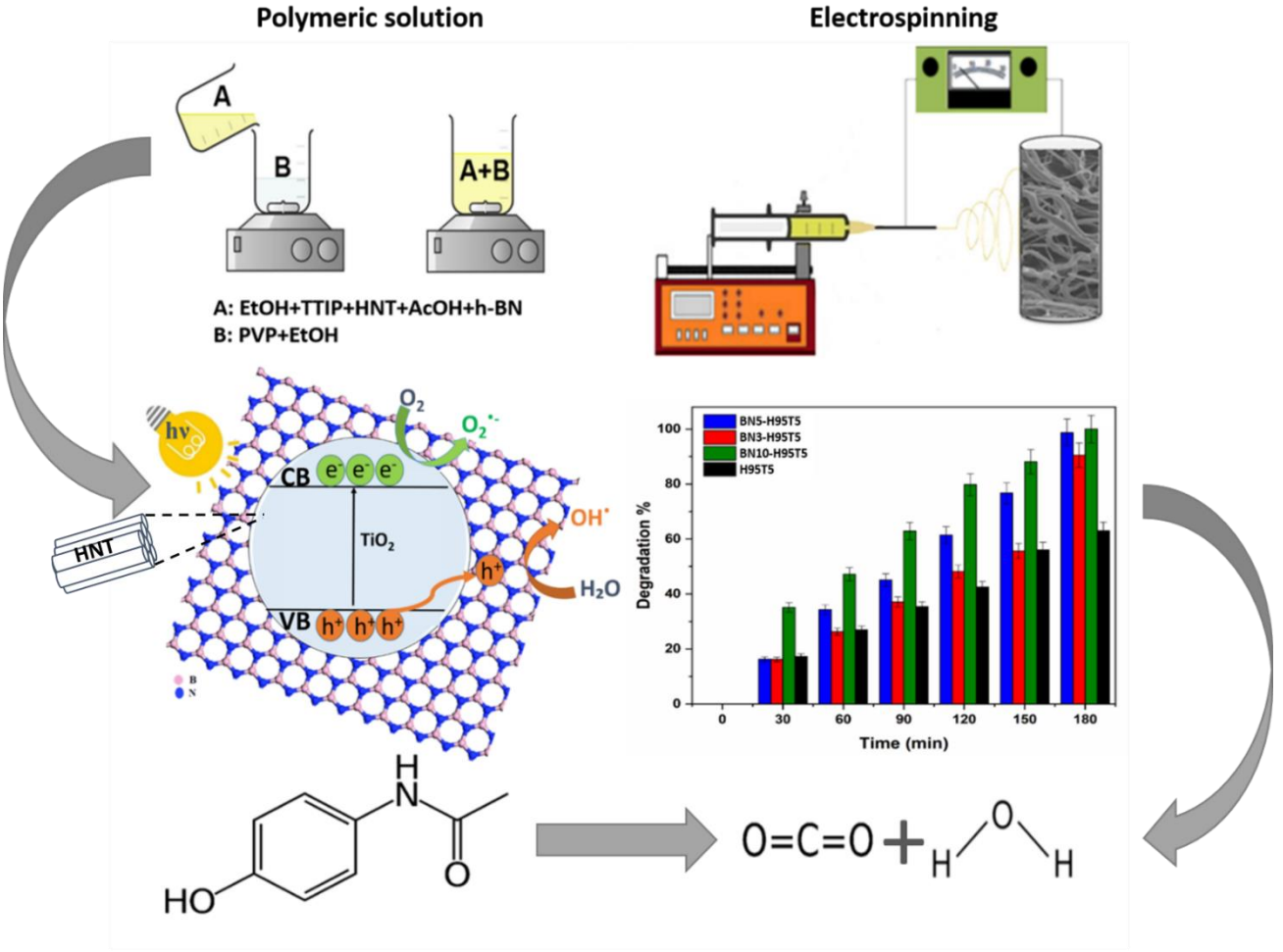

Highlights

1. **Halloysite, titanium oxide, and boron nitride nanosheets were combined to fabricate composite nanofibers.**
2. **Under visible light, these composite nanofibers degraded >98% of acetaminophen after 180 minutes**
3. **The synthesized catalyst remained stable for five cycles.**
4. **$^{\bullet}OH$, h^{+} and $O_2^{\bullet-}$ were mainly implicated in acetaminophen photodegradation.**

1. Introduction

Due to population growth, industrialization, and global development, human activities have grown exponentially with the consumption of many chemicals[1,2]. In many cases, pollutants have been introduced into aquatic resources, such as pharmaceuticals, pesticides, dyes, and personal care products, are considered a new class of pollutants.[3–5] Uncontrolled discharge of untreated water containing these micropollutants form various plants ends up in the environment and results in water pollution[6–8]. The detection of emerging contaminants, even at low concentrations can have adverse effects on human health and a drastic impact on ecosystem. Therefore, these emerging pollutants require the implementation of innovative processes that have been intensively studied over the past few decades.[9–11] Various processes have proven their effectiveness in removing traces of persistent compounds in water, such as reverse osmosis, nanofiltration and advanced oxidation processes (AOP)[12–26]. These technologies have been used in the pre-treatment process and/or post-treatment of conventional wastewater treatment. In recent years, heterogeneous photocatalysis has emerged as a promising technology against water pollution. Applying this process in water treatment, offer the ability of destroying recalcitrant organic pollutants by producing more biologically degradable and less harmful compounds. In this technique, contaminants are destroyed through the combination between light energy and semiconductor photocatalysts. The fundamental principle of photocatalysis is based on the excitation of electron in a semiconductor by the absorption of irradiation to photogenerated carries that will destroy recalcitrant pollutant[14,17–26]. In practice, titanium oxide (TiO_2) is considered the most promising semiconductor oxide for the removal of organic compounds due to its advantages. Nevertheless, it is wide bang gap energy, rapid recombination of electron hole-pair and low conductivity limit its performance in the above processes. There drawbacks could be overcome by forming a heterostructure composite through the combination of TiO_2 with other compounds.[27,28]. Many researchers have tried to reduce its fast electron-hole recombination, which limits the photocatalytic activity[29,30], by producing nanocomposites in which TiO_2 is combined with metal ions (e.g. Pd[31], Ag[32,33], Pt[31,34]), non-metal ions (e.g. B, N, Cu, Ni)[35,36], or semi-conductors (e.g. BN, ZnO, CuO)[37–40]. Boron nitride (BN) has been frequently tested because it has a wide surface area, is chemically stable, and has a wide band gap (>5.5 eV). Recently, Tang *et al.* found that TiO_2 nanoparticles functionalized on high-purity BN nanotubes display improved photocatalytic features due to the strong electrostatic potential of BN nanotubes[41]. Fu *et al.* showed that the photocatalytic removal rates of rhodamine B and methylene blue were 15 and 8 times higher, respectively, with hexagonal BN (h-BN)/TiO_2, fabricated by ball milling, than with TiO_2[42]. Sheng *et al.* reported 3 and 4 times higher photodegradation rates for rhodamine B and methylene blue using h-BN/TiO_2 fabricated with the sol-gel method than for pure TiO_2[43]. Nasr *et al*. found that compared with TiO_2, electrospun BN/TiO_2 increased by 3.8 times methyl orange photocatalytic degradation[37]. Moreover, Lin *et al.* found that ibuprofen adsorption and photocatalytic oxidation by TiO_2/BN progressively increased with higher BN amounts in the composite[43]. Sayegh *et al.* showed that compared with TiO_2, TiO_2/BN/Pd nanofibers improved acetaminophen (ACT) photocatalytic degradation rate (under visible light) by 9 times[39]. These findings demonstrated that BN nanosheets increase TiO_2 photodegradation of pollutants by reducing the electron-hole recombination because holes are attracted to BN.

Recently, we showed that TiO_2-based composite nanofibers with 95% of HNT (i.e. H95T5 composite nanofibers)[44] can degrade 91% of ACT under visible light in 6 hours. Here, we hypothesized that H95T5 photocatalytic activity could be improved by adding BN nanosheets. Therefore, we prepared a novel non-toxic composite nanofibers BN/H95T5 with different BN amounts (0, 3, 5, and 10 wt% of H95T5 mass) by electrospinning. We characterized their structure and morphology using Fourier transform infrared spectroscopy (FT-IR), X-ray diffraction (XRD), scanning and transmission electron microscopy (SEM and TEM), X-ray photoelectron spectroscopy (XPS), Raman and Brunauer-Emmet-Teller analysis (BET). Then, we tested the different composite samples for ACT degradation under visible light, and identified the intermediates and reaction by-products using high-performance liquid chromatography (HPLC). We also performed toxicity screening tests to assess the acute toxicity of by-products formed during ACT degradation, and scavenger tests to determine the reactive species implicated in ACT degradation.

2. Materials and Methods

2.1. Materials

Halloysite was from Tamra (HNT, Nefza District, NW Tunisia) and was purified by sedimentation and sodium exchange modification. BN powder (PHPP325B) was purchased from Saint Gobain (Cavaillon, France) (CAS No. 10043-11-5, 95% purity, 325 mesh, 3µm particle size). Titanium tetraisopropoxide (TTIP, 97 %, CAS: 546-68-9), polyvinyl pyrrolidone (PVP, Mw=1300000, CAS: 9003-39-8), sodium chloride (NaCl, ≥99 %, CAS: 7647-14-5), silver nitrate ($AgNO_3$, >99 %, CAS: 7761-88-8), gelatin from porcine skin (CAS: 9000-70-8), nafion perfluorinated resin solution (CAS: 31175-20-9), ACT (≥99 % CAS: 103-90-2), 2-propanol (IPA, 99.9 %, CAS: 67-63-0), p-benzoquinone (BQ, $C_6H_4O_2$, ≥99.5 %, CAS:106-51-4) and ethylenediaminetetraacetic acid (EDTA, 99.995 %, CAS: 60-00-4) were purchased from Sigma–Aldrich. Acetic acid (≥99 %, CAS: 64-19-7) and ethanol (≥99.8 %, CAS: 64-17-5) were from VWR Chemicals and were used as solvents. The bioluminescent marine bacterium *Vibrio fischeri* LCK 487 was from Hach Lange France SAS. All chemicals were used without further purification. Deionized water (>18.2 MΩ) was produced with the Millipore (Milli-Q® Academic) water purification system.

2.2. BN exfoliation

To prepare exfoliated BN, 20 g of gelatin was added slowly to 80 mL hot water (75°C), and then 1g of BN powder was stirred in at 50°C. After overnight sonication (80% amplitude with pulse off/on 5-10 s) at 50°C using an ultrasonic homogenizer, exfoliated BN was centrifuged at 6000 rpm for 30 minutes, dried at 80°C for 24 hours, and calcined at 600°C for 2 hours[45,46].

2.3. Preparation of H95T5 and BN composite nanofibers

H95T5 nanofibers with/without BN (Table 1) were synthesized by electrospinning. To prepare the solution to be spun, different BN amounts (0, 3, 5, and 10 wt% of H95T5 mass) and 2 ml of absolute ethanol were homogenized for 12h to disperse BN in ethanol, and titanium tetraisopropoxide was resuspended in 2 ml acetic acid and 3 ml ethanol with 0.3 g polyvinylpyrrolidone. The solutions were mixed at room temperature for 1 hour. The

electrospinning set-up and conditions were as previously described.[44] The obtained nanofibers were fully hydrolyzed in air overnight and annealed at 400°C in air for 4 hours.

Table 1. H95T5 and BN/H95T5 samples used in this study.

Sample name	Sample description	BN content (%)
H95T5	H95T5	0
BN3	BN3/H95T5	3
BN5	BN5/H95T5	5
BN10	BN10/H95T5	10
BN	BN	100

2.4. Structural characterization

Scanning (Hitachi S-4800) and transmission electron microscopy (JEOL 2200FS (200 kV)-Japan) and the Brunauer-Emmett-Teller (BET) method with data points and relative pressures (P/Po) from 0 to 1 were used to assess the sample microstructure, phase, crystal structure and their surface and micropore area, respectively. X-ray diffraction (XRD) (PANalytical Xpert-PRO diffractometer with an X'celerator detector and Ni-filtered Cu-radiation) and Raman spectrometry (Horiba Xplora, 532 nm) were used to characterize the sample structure and crystallinity. X-ray photoelectron spectroscopy (XPS) (ESCALAB 250 spectrometer, Thermo Electron, with an Al Kα monochromatic source of 1486.6 eV as excitation source) was used to assess elemental composition and oxidation states.

2.5. Electrochemical activity

Electrodes were prepared by dissolving each sample (5 mg) in 1 mL isopropanol/40 µL Nafion with sonication for 30 minutes. The obtained slurry was deposited on ITO glass (60 mm x 21mm x 2 mm) (4 cm^2 coverage), and films were dried at room temperature.

Electrochemical impedance was measured with a Solartron SI 1287 galvanostatic-potentiostat and a three-electrode system in which Ag/AgCl was the reference electrode, platinum wire the counter electrode, and 0.1 M Na_2SO_4 the electrolyte. Measurements were performed at room temperature, first in the dark and then under visible light (150 W linear halogen lamp with a visible light source range = 420–600 nm). The lamp-quartz window distance was 10 cm and the power density was 8.2 mW/cm^2. Data were recorded at 0.4-0.6V [47].

2.6. Photocatalytic activity

ACT degradation (10 ppm in aqueous solution) upon visible light (linear halogen lamp, 400W, Avide) exposure was quantified to determine the photocatalytic activity of the different composite nanofibers. Each photocatalyst (0.5 g/L) was dispersed in the aqueous solution by sonication in the dark for 30 min to reach the adsorption-desorption equilibrium. All experiments were carried out in the same conditions: lamp-solution distance of 10 cm and temperature of 25°C (maintained by circulating water in the cylindrical tube that surrounded

the photoreactor). During visible light exposure, 2-ml aliquots were taken every 30 minutes and filtered with 0.45 μm filters. HPLC with a C-18 column (RP18, Nucleoshell) and a Quattro-Micro mass spectrometer with an electrospray probe (Waters Micromass, Wythenshawe, Manchester, UK) as detector was used to identify intermediates and reaction products.

Each sample photocatalytic activity was calculated as the percentage of ACT degradation[48]:

$$\text{Degradation efficiency (\%)} = [(C_0\text{-}C)/C_0] \text{ x}100 \qquad (1)$$

where C_0 and C are ACT concentrations before and after exposure to visible light.

2.7. Photocatalytic degradation kinetics

ACT concentration changes during photocatalytic degradation were modeled using a pseudo-first-order kinetic model and equation *2*[49]:

$$\ln (C_0/C) = K_{app}\, t \qquad (2)$$

where C_o is the initial concentration, C the concentration at the time t, and K_{app} is the apparent rate constant.

2.8. Toxicity tests

To assess the toxicity of the solution aliquots collected during ACT photodegradation, micro-toxicity tests were done using *Vibrio fischeri* LCK 487 as previously described [44].

3. Results and Discussion

3.1. Morphology and structure of H95T5 nanofiber samples with and without BN

The scanning electron microscopy-based morphological analysis of the H95T5, BN3, and BN5 samples **(Table 1)** showed uniform, continuous and randomly oriented nanofibers (**Fig. 1a-c**). Their mean diameter increased slightly from (233 ± 10nm) for H95T5 to (256 ± 10nm) and (283 ± 10nm) for BN3 and BN5, respectively. This confirmed the inclusion of BN nanosheets[37,44,50]. Conversely, in BN10, nanofibers were not homogenous (**Fig. 1d**), and nanofibers with two size ranges, possibly linked to different concentration and agglomeration of BN nanosheets, were observed. Therefore, the subsequent characterization focused mainly on samples with 5% BN.

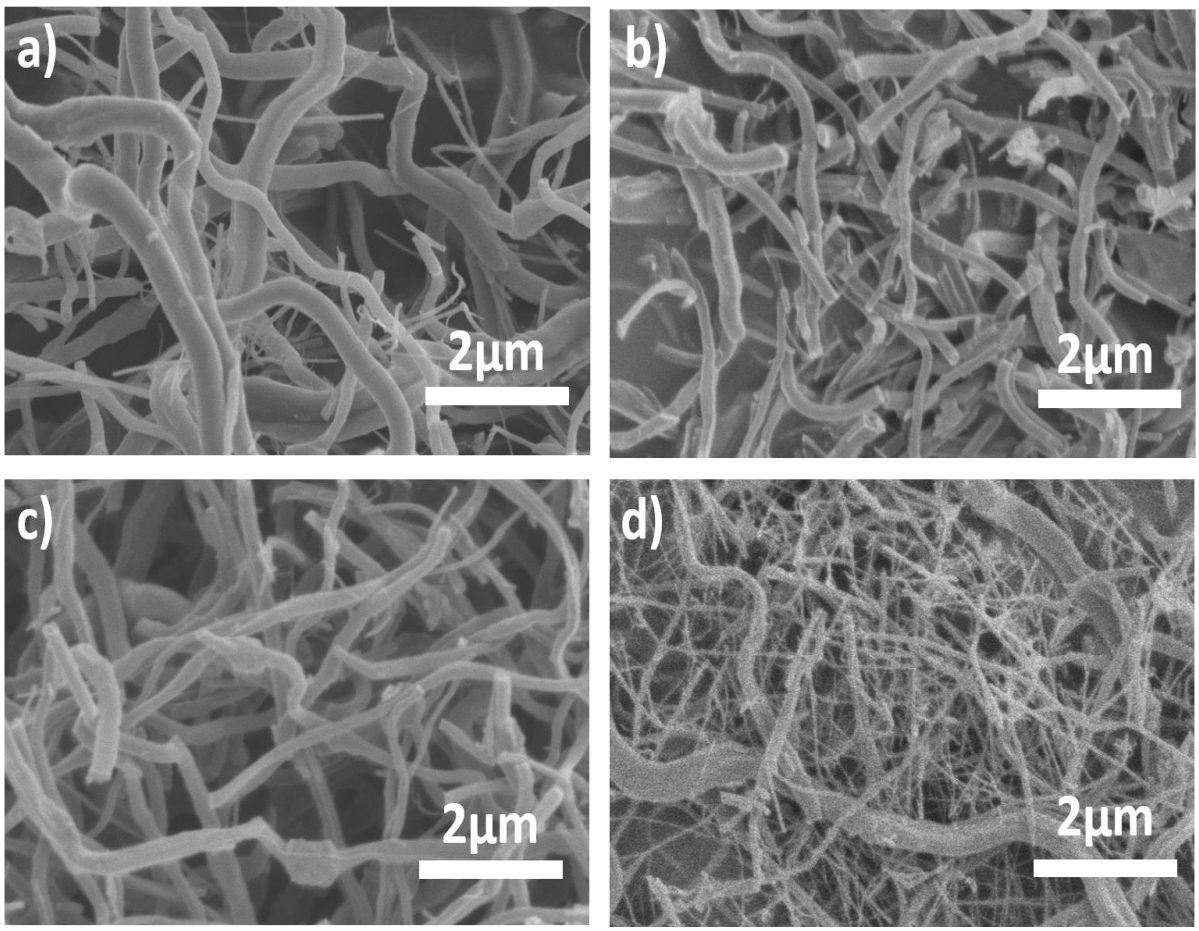

Fig. 1. Scanning electron microscopy photographs of H95T5 (a), BN3 (b), BN5 (c), and BN10 (d) (described in Table 1).

The XRD patterns of the H95T5, BN3, BN5, BN10 samples at 2θ (to investigate their crystallinity) **(Fig. 2a)** contained the 001 reflection of HNT (7.18 Å), and TiO_2 anatase phase with tetragonal arrangement reflections at 2θ=25.3, 37.9, 48.0, 54.0, 55.2, 62.5, 68.9, 69.9 and 75.07° attributed to the (101), (112), (200), (105), (211), (204), (116), (220), and (215) Miller plans, respectively[44,51,52]. Upon BN addition, the main TiO_2 reflection was shifted (**Fig. 2b**), the lattice strain in the TiO_2 cell was increased, the formation of self-trapped excitons was decreased, and vacancies in the TiO_6 octahedral were created.[53]

FT-IR spectroscopy confirmed the presence of functional groups in the different samples (**Fig. 2c-d**). The two peaks at 3694 and 3617 cm^{-1} and the band at 907 cm^{-1} were attributed to the stretching and deformation vibrations of inner-surface hydroxyl groups, respectively[44]. The absorption band at 650–800 cm−1 was due to Ti–O bonds. The two peaks at ~800 and 1370 cm^{-1} were identified as the two main absorption peaks of hBN (B–N–B and B–N) and their intensity increased for samples with progressively higher BN amounts[44,46,54].

Raman spectroscopy (recorded from 50 to 1500 cm^{-1}) showed the presence of six Raman active modes (A1g, 2 B1g, 3Eg) that corresponded to the pure anatase phase of TiO_2 (**Fig. 2e**). The Raman spectra of BN/H95T5 samples included the peak for hBN at ~1369 cm^{-1}, referring to the E2g mode of BN **(Fig. 2f)**. The intensity of this peak increased with the BN amount in the sample, in agreement with the XRD and FTIR findings, thus confirming BN incorporation in the BN/H95T5 nanocomposites[44,53].

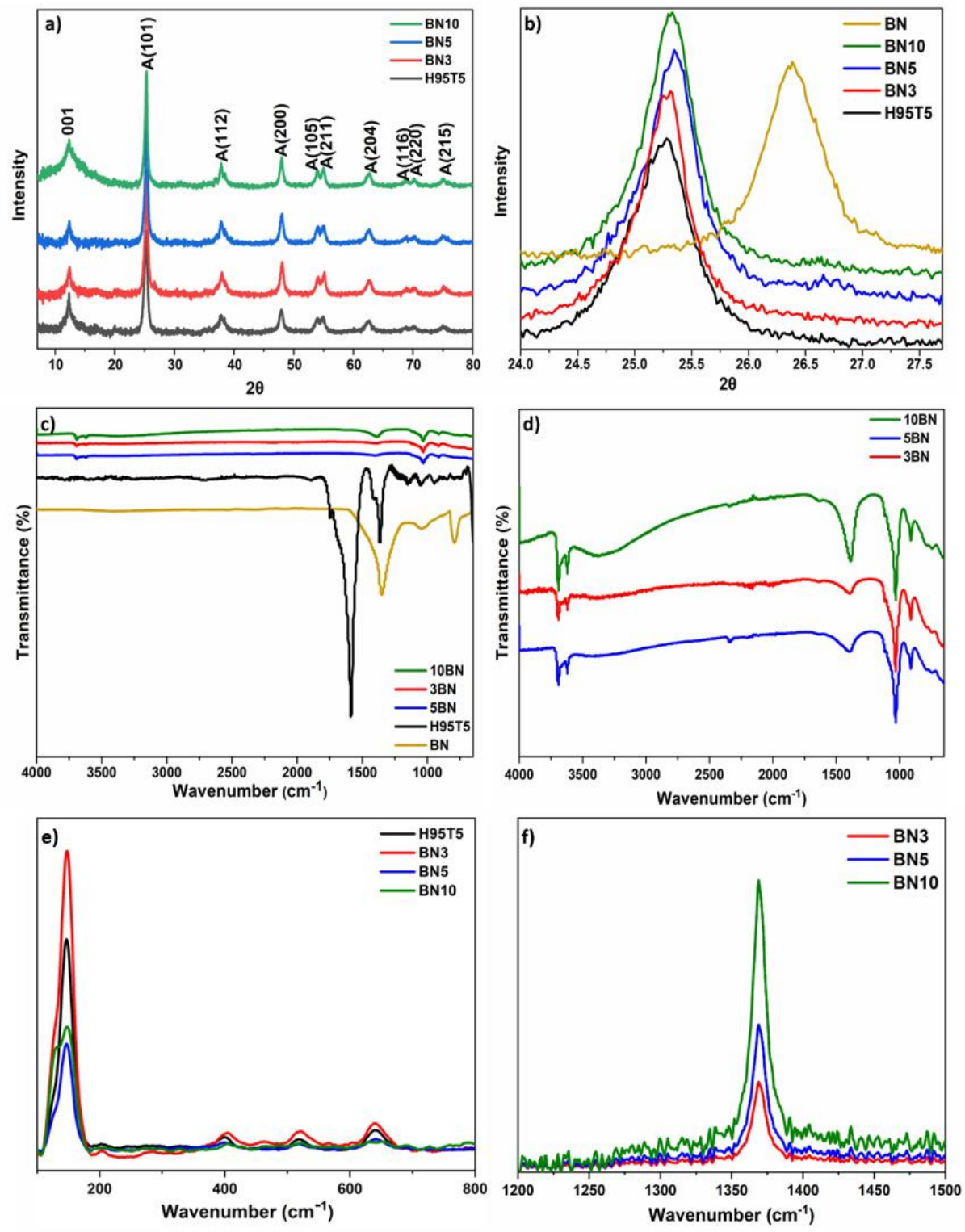

Fig. 2. XRD profiles (a,b), FT-IR spectra (c-d), and Raman spectra (e-f) of H95T5, BN3, BN5 and BN10 nanocomposite fibers.

The nanocomposite structure was then analyzed by high-resolution transmission electron microscopy showing the similarity of the BN5 and H95T5 surfaces (**Fig. 3a-e**). Both samples had a rough and large surface area with a lattice spacing of 0.350 nm, in agreement with the distance of the (101) crystalline plane of anatase TiO_2.[44] In BN5, the lattice spacing (0.337 nm) corresponded to the typical (002) diffraction peak of BN.[55]

Scanning transmission electron microscopy of BN5 showed that Ti, Si, Al, B, and N atoms were homogeneously distributed **(Fig. 3g)** and that Al–K, Si-K, B-K, and N-K were inside the nanofibers, thus proving BN and HNT dispersion in the nanofibers.

Then, XPS was used to analyze the surface structure and chemical state of each element in the BN/H95T5 nanocomposites.

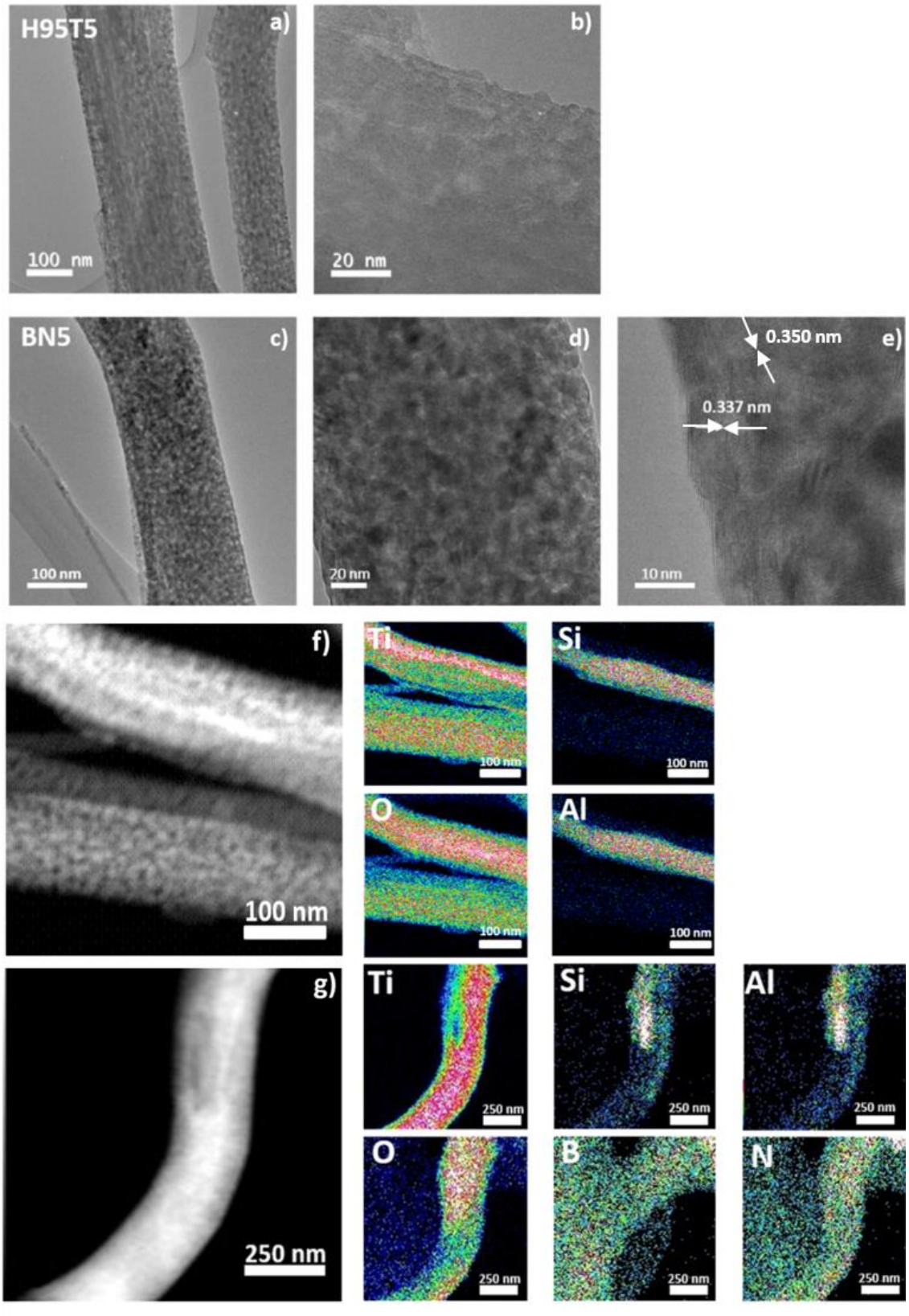

Fig. 3. Transmission electron microscopy (TEM) photographs of H95T5 (a,b) and BN5 (c-e) and chemical mapping of H95T5 (f) and BN5 (g) by scanning TEM-energy dispersive X-ray spectroscopy.

The signal intensity in the XPS survey spectrum for BN5 (**Fig. 4a**) was strong for Ti 2p and O 1s, and weak for C 1s, Al 2p, Si 2p, N 1s, and B. For H95T5, two peaks were observed at 458.5 and 464.2 eV (i.e. the Ti $2p_{3/2}$ and Ti $2p_{1/2}$ states attributed to Ti^{4+})[23] (data not shown). In BN5, the binding energy of these two peaks was slightly increased (+0.2 eV) (**Fig. 4b**) due to BN inclusion in the TiO_2 lattice and the formation of oxygen vacancies that have a high electronegativity effect by promoting the formation of Ti^{3+} centers in the TiO_2 lattice.[56] The O 1s spectrum had three peaks at 530.1, 531.1, and 532.7 eV that were attributed to Ti-O-N, B-O-H, and B-O-Ti (**Fig. 4c**). In the B 1s spectrum (**Fig. 4e**), the peaks at 190.57, 191.67, and 193.37 eV were assigned to B–N, B–OH, and B–OTi, respectively. Deconvolution of the N 1s peaks (**Fig. 4d**) showed the presence of two peaks at 397.9 and 399.8 eV ascribed to B–N and N–O–Ti, as already seen in the O1 s and B 1s spectra[36–38]. These findings confirmed that BN had been incorporated in the TiO_2 lattice and was homogeneously dispersed in the nanofibers.

Moreover, the specific surface areas of H95T5 and B5, calculated with the BET method, were 36.6 m^2/g and 59.9 m^2/g. This surface area increase was explained by BN sheet incorporation in TiO_2 nanofibers and should enhance the photocatalytic activity by creating new active adsorption sites[35].

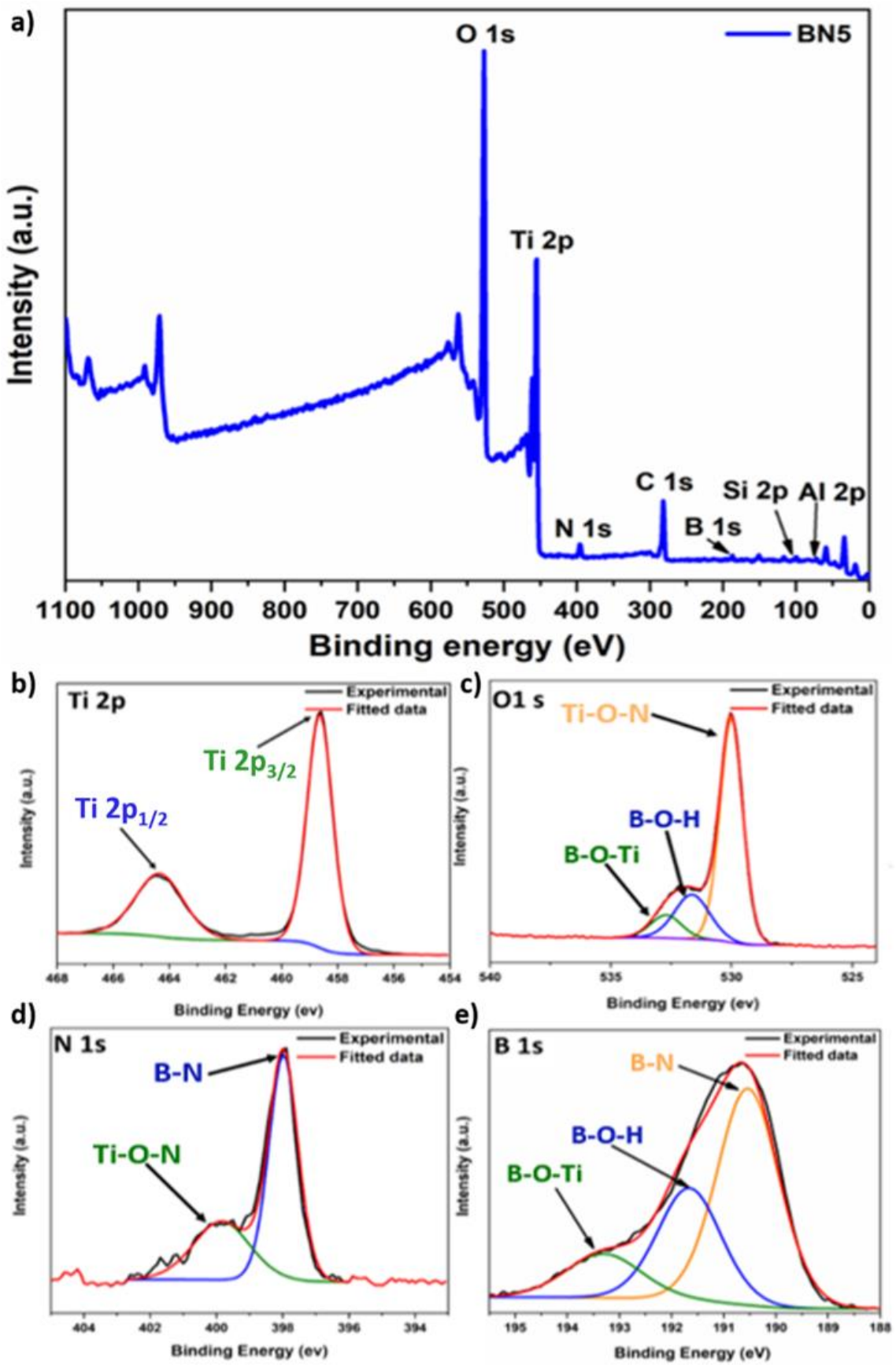

Fig. 4. XPS analysis of BN5 chemical state: (a) survey, (b) Ti 2p, (c) O 1s, (d) N 1s, and (e) B 1s spectra.

3.2. Electrochemical activity

BN5 photo-induced charge separation efficiency and transmission rate were determined using electrochemical impedance spectroscopy with same model as stated before[44]. In the dark, BN5 showed a faster charge transfer rate than H95T5 (**Fig. 5a**). After visible light irradiation, the Nyquist curves (**Fig. 5b**) showed that resistance increased from 1280 Ω with H95T5 to 1563 Ω with BN5, indicating lower electron-hole pair recombination.

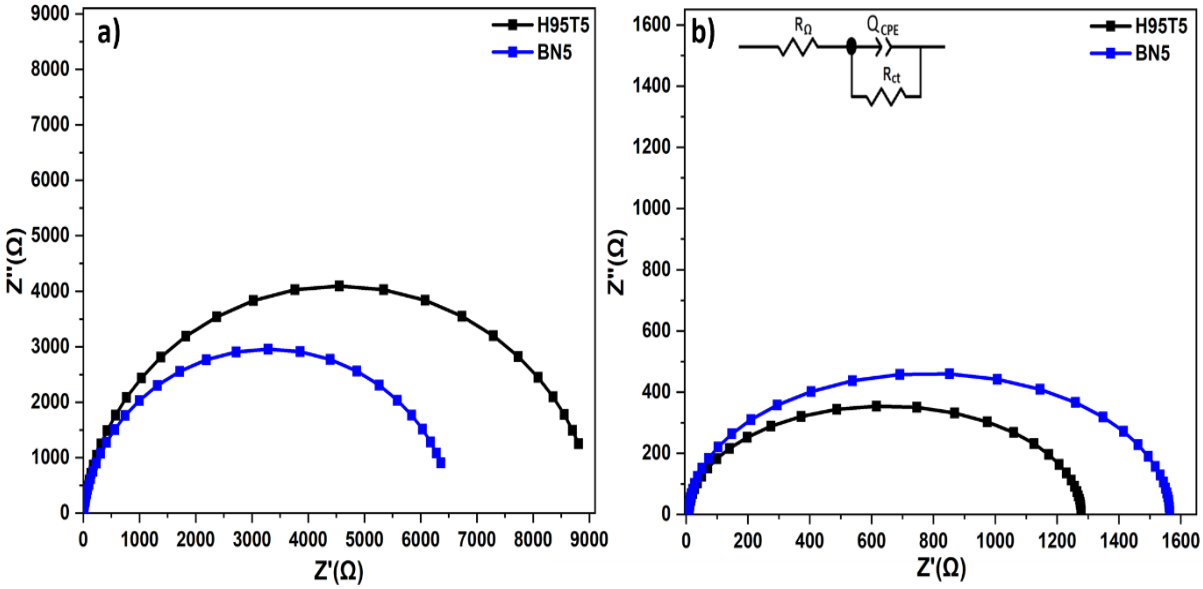

Fig. 5. Nyquist curves of H95T5 (black) and BN5 (blue) in the dark (a) and in the presence of visible light (b). The inset shows the proposed circuit.

The presence of drugs in aquatic environment is recognized as hazardous emerging contaminants due to their persistence, bioaccumulation in life form and toxicological profile[57]. Their quantification shows that they can be found in nature in very low concentration (ng.L^{-1} and µg.L^{-1}). However, the exposure to trace concentrations of pharmaceuticals in drinking water even at these levels could affect adversely human health and wildlife[58]. Among the drugs, acetaminophen (ACT) also known as paracetamol is considered the most significant due to its use and consumption in both human medicine and veterinary[59,60]. Our aim objective in this context, is to evaluate the efficiency of this composite in the degradation of ACT in neutral aqueous solution. By the fact that acetaminophen is easily dissolved in water, our study was restricted on the use of aqueous solution at neutral pH.

ACT degradation was quantified during 3 hours of visible light irradiation by H95T5 and BN composites. Moreover, ACT cannot be easily photodegraded without a catalyst[44]. At the end of the experiment, ACT degradation rate was higher when samples with higher BN concentrations were used 63% with H95T, 90% with BN3, 99% with BN5, and 100% with BN10 (**Fig. 6a**). This showed that doping with BN nanosheets facilitates electron-hole pair separation due to electrostatic interactions. This could be due to promotion of electron transfer from activated TiO_2 to the BN nanosheets thanks to the negatively charged surface of BN nanosheets [42,61]. Thus, in the BN-doped samples more photoelectrons were available, compared with H95T5, for ACT photodegradation. Moreover, BN nanosheet adsorption of hydrophilic molecules from the aqueous solution is reduced due to its hydrophobic surface[62,63].

Table 2 shows that despite the low BN quantity in our BN/H95T5 composite nanofibers, their degradation performances were comparable to those of previously described photocatalysts.

A pseudo first-order reaction could model ACT degradation kinetics in the presence of visible light due to the curve linearity and the linear coefficient R^2 close to 1 (**Fig. 6b).** ACT degradation rates were higher with BN/H95T5 composite nanofibers than with H95T5 due to the formation of heterojunctions in the presence of BN.

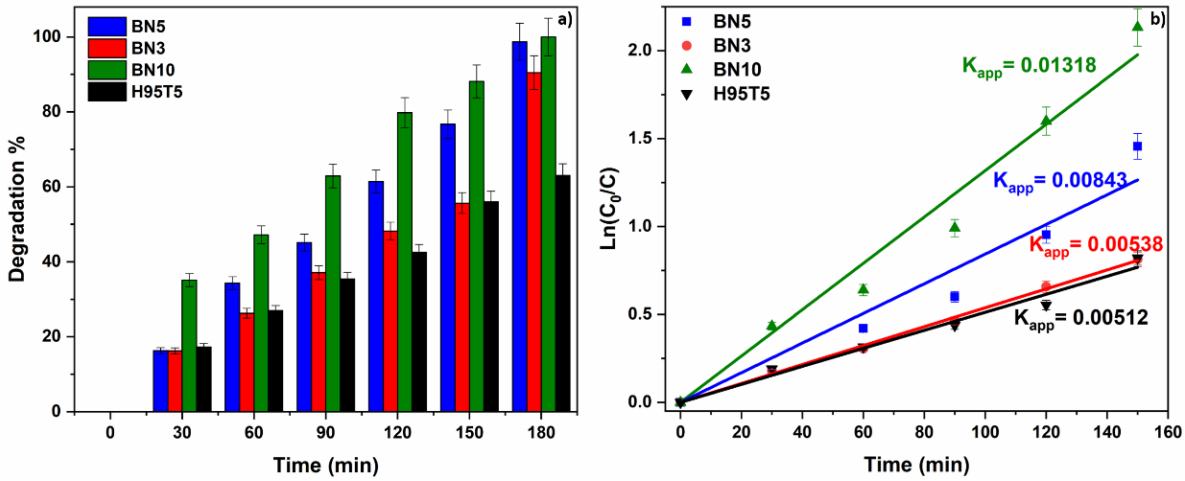

Fig. 6. ACT degradation under visible light (a) and kinetics of ACT photocatalytic degradation (b) using the indicated samples as catalyst. Data are the mean of three measurements and the relative error was lower than ±5%.

For the next experiments, BN5 was selected (rather than BN10) because it was cheaper (less BN required) and showed homogenous nanofiber distribution (see scanning electron microscopy data, Fig. 1). BN5 stability over 5 cycles was tested using 10 mg/L ACT at pH 7 and the B5 sample was filtered, washed in deionized water, and dried at 100°C for 12h before the next cycle. No loss of catalytic activity was observed after five cycles (**Fig. 7a**), indicating that doping with BN nanosheets improves the catalyst stability.

Then, EDTA, p-benzoquinone, and isopropanol were used as scavengers (0.06M[64]) to identify the reactive radicals implicated in ACT photodegradation. Each scavenger was added to the ACT solution before exposure to visible light[65], followed by aliquot collection at specific time points to quantify ACT concentration. ACT degradation was completely inhibited by EDTA (h^+ radical scavenger) (**Fig. 7b**), highlighting the key implication of h^+ radicals. In the presence of isopropanol ($^{\bullet}OH$ scavenger), only 45% of ACT was degraded, indicating that $^{\bullet}OH$ radicals contribute to ACT degradation. Addition of p-benzoquinone inhibited ACT degradation by ~80%, showing that $O_2^{\bullet-}$ are strongly implicated[39]. In conclusion, ACT photodegradation requires the presence of $^{\bullet}OH$, h^+, and $O_2^{\bullet-}$ radicals[39].

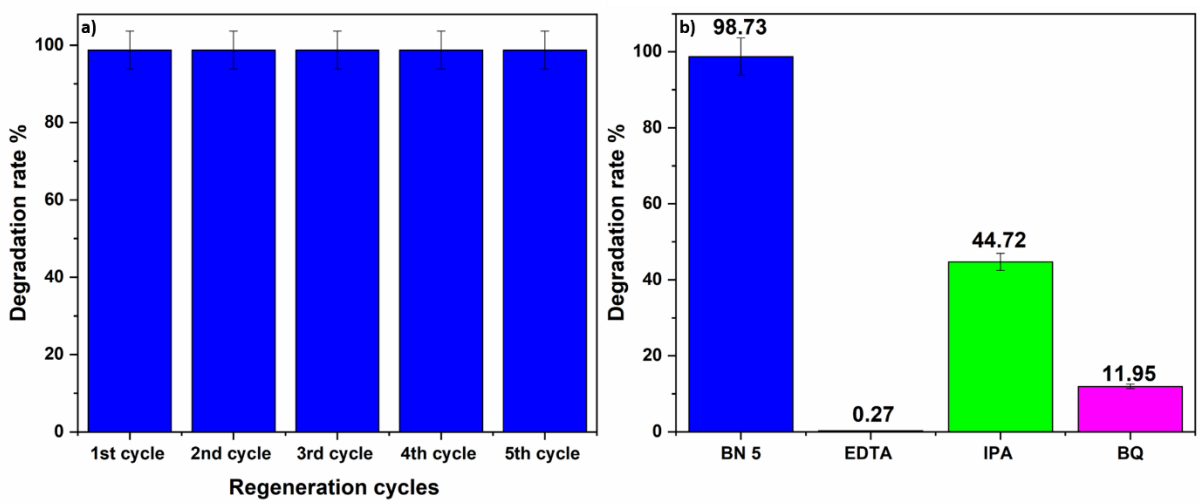

Fig. 7. BN5 stability (a); effect of the indicated scavengers on ACT photodegradation by BN5 (b). EDTA, ethylenediaminetetraacetic acid; IPA, isopropanol; BQ, p-benzoquinone.

Acute toxicity assays showed that in the solution that contained BN5 and ACT and in the presence of visible light, *V. fischeri* fluorescence was progressively inhibited: 27% after 15 min and up to 85% after 2 hours. This indicated that toxic aromatic by-products are produced during ACT photocatalytic degradation (**Fig. 8a**). The progressive decrease of this effect (from 82% of fluorescence inhibition after 6 hours to 5% after 24 hours) showed that both ACT and toxic by-products were degraded by BN5 upon exposure to visible light. HPLC analysis of the different aliquots showed the formation of toxic aromatic molecules (e.g. 1,4-benzoquinone, benzoic acid, benzaldehyde) that after the first 2 hours, started to be metabolized into non-toxic compounds, such as carboxylic acids (e.g. maleic acid, oxalic acid)[49,66,67].

These findings allowed proposing a model to explain the generation of oxidants and ACT photodegradation by BN5 (**Fig. 8b**). First, hydroxyl radicals ($^{\bullet}OH$) and superoxide radical anions ($O_2^{\bullet-}$) are produced following the formation of electron-hole (e-/ h^+) pairs by TiO_2 and HNT. The production of ($^{\bullet}OH$) allows ACT mineralization. Upon BN inclusion in BN5, B–O–Ti bonds are formed that cause the disturbance of charge balance by oxygen holes, thus affecting the capture of photogenerated electrons. These electrons can be moved to the π–π conjugate system of BN, thus hampering electron-hole pair recombination. This contributes to increasing BN5 photocatalytic activity and participating in ACT mineralization into CO_2 and H_2O.

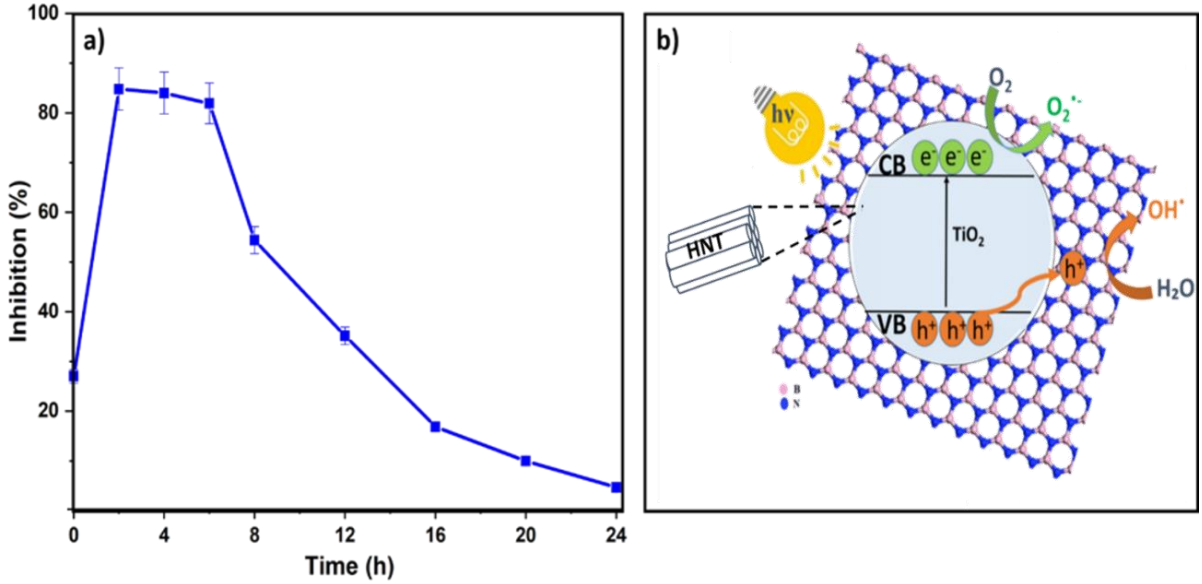

Fig. 8. Monitoring *Vibrio fischeri* luminescence changes when in contact with ACT and BN5 (a); model describing how BN5 catalyzes ACT degradation in the presence of visible light (b).

Table 2. BN5, H95T5, and other photocatalysts (previous studies) used to degrade water pollutants

Pollutant (mg/L)	Photocatalyst (g/L)	Synthesis method	Irradiation type	Removal efficiency (%)	Degradation time (min)	Ref.
ACT (10 mg/L)	BN5	Sol-gel + Electrospinning	Halogen linear lamp	99	180	This work
ACT (10 mg/L)	H95T5 (0.5 g/L)	Sol-gel + Electrospinning	Halogen linear lamp	91	360	[44]
ACT (1 mg/L)	TiO_2–BN100–Pd100	Atomic layer deposition + Electrospinning	Halogen linear lamp	98	180	[39]
Methylene blue (10 mg/L)	BN/TiO_2 (0.33 g/L)	Ice bath method	Visible light	79	200	[68].
Rhodamine B (10mg/L)	12 wt% BN/TiO_2 (0.5 g/L)	Solvothermal method	Visible-light Xe lamp	99	150	[69]
Rhodamine B (10 mg/L)	12% h-BN/TiO_2 (0.75 g/L)	Solvothermal method	Visible light	95	120	[70]
Ibuprofen (5 mg/L)	TiO_2–10% BN (0.2 g/L)	Sol-gel + Electrospinning	Halogen linear lamp	100	120	[71]
Methyl orange (10mg/L)	TiO_2–10% BN (0.4 g/L)	Sol-gel + Electrospinning	Visible light irradiation	99	75	[37]
Methylene blue (20 mg/L)	BN(5 wt%)–Ag(3 wt%)/TiO_2	Sol-gel + Electrospinning	Visible light irradiation	98	80	[32]

Conclusion

In this study, a novel non-toxic composites (BN/H95T5) with different amounts of BN nanosheets were fabricated by combining sol-gel and electrospinning. HNT structure was maintained by annealing at 400 °C. Characterization of these nanofibers showed BN presence in the nanofiber (XRD and Raman spectroscopy), good HNT and BN dispersion (TEM), Ti $2p_{1/2}$, Ti $2p_{3/2}$, B-N, and N-O-Ti presence (XPS) and the formation of oxygen vacancies with high electron-attracting effect. Moreover, resistance was higher following BN incorporation due to the reduced e^-/h^+ recombination (electrochemical impedance spectroscopy). ACT degradation was two times faster in the presence of BN5 nanofibers than H95T5 nanofibers. Due to electrostatic interactions, the naturally negatively charged surface of BN nanosheets could transfer h^+ from the activated TiO_2 surface to BN sheets. BN5 catalytic performance remained stable during five consecutive cycles. Quenching and toxicity (*V. fischeri*) assays indicated that ACT photodegradation was mainly catalyzed by $^{\bullet}OH$, h^+, and $O_2^{\bullet-}$ radicals and that toxic aromatic by-products were formed, but then transformed into non-toxic compounds. Overall, this nanocomposite with low TiO_2 and BN concentrations is a candidate for cheap mass production of a photocatalyst for water pollutant removal.

Acknowledgements

This study was possible thanks to the H2020-MSCA-RISE-2017 project, 'Novel 1D photonic metal oxide nanostructures for early stage cancer detection' (Project number: 778157). I.I. was partly funded by the NCN SONATA-BIS program (UMO-2020/38/B/ST5/00176). M.A. was financially supported by the Tunisian Ministry of Higher Education and Scientific Research.

Reference

(1) Mekonnen, M. M.; Hoekstra, A. Y. Four Billion People Facing Severe Water Scarcity. *Sci. Adv.* **2016**, *2* (2), e1500323. https://doi.org/10.1126/sciadv.1500323.

(2) Committee on the Review of Environmental Protection Agency's Science to Achieve Results Research Grants Program; Board on Environmental Studies and Toxicology; Division on Earth and Life Studies; National Academies of Sciences, Engineering, and Medicine. *A Review of the Environmental Protection Agency's Science to Achieve Results Research Program*; National Academies Press: Washington, D.C., 2017; p 24757. https://doi.org/10.17226/24757.

(3) Akash, S.; Sivaprakash, B.; Rajamohan, N.; Govarthanan, M.; Elakiya, B. T. Remediation of Pharmaceutical Pollutants Using Graphene-Based Materials - A Review on Operating Conditions, Mechanism and Toxicology. *Chemosphere* **2022**, *306*, 135520. https://doi.org/10.1016/j.chemosphere.2022.135520.

(4) Vaudreuil, M.-A.; Vo Duy, S.; Munoz, G.; Sauvé, S. Pharmaceutical Pollution of Hospital Effluents and Municipal Wastewaters of Eastern Canada. *Sci. Total Environ.* **2022**, *846*, 157353. https://doi.org/10.1016/j.scitotenv.2022.157353.

(5) Li, W. C. Occurrence, Sources, and Fate of Pharmaceuticals in Aquatic Environment and Soil. *Environ. Pollut.* **2014**, *187*, 193–201. https://doi.org/10.1016/j.envpol.2014.01.015.

(6) Varsha, M.; Senthil Kumar, P.; Senthil Rathi, B. A Review on Recent Trends in the Removal of Emerging Contaminants from Aquatic Environment Using Low-Cost Adsorbents. *Chemosphere* **2022**, *287*, 132270. https://doi.org/10.1016/j.chemosphere.2021.132270.

(7) *Water Remediation*; Bhattacharya, S., Gupta, A. B., Gupta, A., Pandey, A., Eds.; Energy, Environment, and Sustainability; Springer Singapore: Singapore, 2018. https://doi.org/10.1007/978-981-10-7551-3.

(8) Muñiz-Bustamante, L.; Caballero-Casero, N.; Rubio, S. Drugs of Abuse in Tap Water from Eight European Countries: Determination by Use of Supramolecular Solvents and Tentative Evaluation of Risks to Human Health. *Environ. Int.* **2022**, *164*, 107281. https://doi.org/10.1016/j.envint.2022.107281.

(9) Ma, D.; Yi, H.; Lai, C.; Liu, X.; Huo, X.; An, Z.; Li, L.; Fu, Y.; Li, B.; Zhang, M.; Qin, L.; Liu, S.; Yang, L. Critical Review of Advanced Oxidation Processes in Organic Wastewater Treatment. *Chemosphere* **2021**, *275*, 130104. https://doi.org/10.1016/j.chemosphere.2021.130104.

(10) Bethi, B.; Sonawane, S. H.; Bhanvase, B. A.; Gumfekar, S. P. Nanomaterials-Based Advanced Oxidation Processes for Wastewater Treatment: A Review. *Chem. Eng. Process. - Process Intensif.* **2016**, *109*, 178–189. https://doi.org/10.1016/j.cep.2016.08.016.

(11) Camargo-Perea, A. L.; Rubio-Clemente, A.; Peñuela, G. A. Use of Ultrasound as an Advanced Oxidation Process for the Degradation of Emerging Pollutants in Water. *Water* **2020**, *12* (4), 1068. https://doi.org/10.3390/w12041068.

(12) Wu, R.; Tan, Y.; Meng, F.; Zhang, Y.; Huang, Y.-X. PVDF/MAF-4 Composite Membrane for High Flux and Scaling-Resistant Membrane Distillation. *Desalination* **2022**, *540*, 116013. https://doi.org/10.1016/j.desal.2022.116013.

(13) Weng, C.; Sun, X.; Han, B.; Ye, X.; Zhong, Z.; Li, W.; Liu, W.; Deng, H.; Lin, Z. Targeted Conversion of Ni in Electroplating Sludge to Nickel Ferrite Nanomaterial with Stable Lithium Storage Performance. *J. Hazard. Mater.* **2020**, *393*, 122296. https://doi.org/10.1016/j.jhazmat.2020.122296.

(14) Luo, G.; Xie, J.; Liu, J.; Zhang, Q.; Luo, Y.; Li, M.; Zhou, W.; Chen, K.; Li, Z.; Yang, P.; Zhao, L.; Siong Teh, K.; Wang, X.; Dong, L.; Maeda, R.; Jiang, Z. Highly Conductive, Stretchable, Durable, Breathable Electrodes Based on Electrospun Polyurethane Mats Superficially Decorated with Carbon Nanotubes for Multifunctional Wearable Electronics. *Chem. Eng. J.* **2023**, *451*, 138549. https://doi.org/10.1016/j.cej.2022.138549.

(15) Han, M.-C.; Cai, S.-Z.; Wang, J.; He, H.-W. Single-Side Superhydrophobicity in Si3N4-Doped and SiO2-Treated Polypropylene Nonwoven Webs with Antibacterial Activity. *Polymers* **2022**, *14* (14), 2952. https://doi.org/10.3390/polym14142952.

(16) Huo, J.; Wei, H.; Fu, L.; Zhao, C.; He, C. Highly Active Fe36Co44 Bimetallic Nanoclusters Catalysts for Hydrolysis of Ammonia Borane: The First-Principles Study. *Chin. Chem. Lett.* **2023**, *34* (2), 107261. https://doi.org/10.1016/j.cclet.2022.02.066.

(17) Bahadoran, A.; Khoshnoudi Jabarabadi, M.; Hameed Mahmood, Z.; Bokov, D.; Jushi Janani, B.; Fakhri, A. Quick and Sensitive Colorimetric Detection of Amino Acid with Functionalized-Silver/Copper Nanoparticles in the Presence of Cross Linker, and Bacteria Detection by Using DNA-Template Nanoparticles as Peroxidase Activity. *Spectrochim. Acta. A. Mol. Biomol. Spectrosc.* **2022**, *268*, 120636. https://doi.org/10.1016/j.saa.2021.120636.

(18) Lin, H.; Li, T.; Janani, B. J.; Fakhri, A. Fabrication of Cu2MoS4 Decorated WO3 Nano Heterojunction Embedded on Chitosan: Robust Photocatalytic Efficiency, Antibacterial Performance, and Bacteria Detection by Peroxidase Activity. *J. Photochem. Photobiol. B* **2022**, *226*, 112354. https://doi.org/10.1016/j.jphotobiol.2021.112354.

(19) Xiao, S.; Fakhri, A.; Janani, B. J. Synthesis of Spinel Tin Ferrite Decorated on Bismuth Ferrite Nanostructures for Synergetic Photocatalytic, Superior Drug Delivery, and Antibacterial Efficiencies. *Surf. Interfaces* **2021**, *27*, 101490. https://doi.org/10.1016/j.surfin.2021.101490.

(20) Mao, Y.; Qiu, J.; Zhang, P.; Fei, Z.; Bian, C.; Janani, B. J.; Fakhri, A. A Strategy of Silver Ferrite/Bismuth Ferrite Nano-Hybrids Synthesis for Synergetic White-Light Photocatalysis, Antibacterial Systems and Peroxidase-like Activity. *J. Photochem. Photobiol. Chem.* **2022**, *426*, 113756. https://doi.org/10.1016/j.jphotochem.2021.113756.

(21) Bahadoran, A.; Baghbadorani, N. B.; De Lile, J. R.; Masudy-Panah, S.; Sadeghi, B.; Li, J.; Ramakrishna, S.; Liu, Q.; Janani, B. J.; Fakhri, A. Ag Doped Sn3O4 Nanostructure and Immobilized on Hyperbranched Polypyrrole for Visible Light Sensitized Photocatalytic, Antibacterial Agent and Microbial Detection Process. *J. Photochem. Photobiol. B* **2022**, *228*, 112393. https://doi.org/10.1016/j.jphotobiol.2022.112393.

(22) Long, W.; Hamza, M. U.; Abdul-Fattah, M. N.; Rheima, A. M.; Ahmed, Y. M.; Fahim, F. S.; Altimari, U. S.; Aldulaim, A. K. O.; Janani, B. J.; Fakhri, A. Preparation, Photocatalytic and Antibacterial Studies on Novel Doped Ferrite Nanoparticles: Characterization and Mechanism Evaluation. *Colloids Surf. Physicochem. Eng. Asp.* **2022**, *650*, 129468. https://doi.org/10.1016/j.colsurfa.2022.129468.

(23) Lai, Y.; Fakhri, A.; Janani, B. J. Synergistic Activities of Silver Indium Sulfide/Nickel Molybdenum Sulfide Nanostructures Anchored on Clay Mineral for Light-Driven Bactericidal

Performance, and Detection of Uric Acid from Gout Patient Serum. *J. Photochem. Photobiol. B* **2022**, *234*, 112526. https://doi.org/10.1016/j.jphotobiol.2022.112526.

(24) Hu, B.; Cui, Y.; Yang, X.; Xu, X.; Janani, B. J.; Fakhri, A. Fabrication of Novel Rational Ti-Sn Doped Cu-Ferrite Nanoparticles for Robust Photocatalysis Reaction, Magnetic Resonance Imaging, and Chemo-Magneto-Photo-Thermal Therapy. *Surf. Interfaces* **2022**, *33*, 102226. https://doi.org/10.1016/j.surfin.2022.102226.

(25) Lei, C.; Sun, N.; Wu, H.; Zhao, Y.; Yu, C.; Janani, B. J.; Fakhri, A. Bio-Photoelectrochemical Degradation, and Photocatalysis Process by the Fabrication of Copper Oxide/Zinc Cadmium Sulfide Heterojunction Nanocomposites: Mechanism, Microbial Community and Antifungal Analysis. *Chemosphere* **2022**, *308*, 136375. https://doi.org/10.1016/j.chemosphere.2022.136375.

(26) Liu, Z.; Hadi, M. A.; Aljuboory, D. S.; Ali, F. A.; Jawad, M. A.; AL-Alwany, A.; Hadrawi, S. K.; Mundher, T.; Riadi, Y.; Amer, R. F.; Fakhri, A. High Efficiency of Ag0 Decorated Cu2MoO4 Nanoparticles for Heterogeneous Photocatalytic Activation, Bactericidal System, and Detection of Glucose from Blood Sample. *J. Photochem. Photobiol. B* **2022**, *236*, 112571. https://doi.org/10.1016/j.jphotobiol.2022.112571.

(27) Moma, J.; Baloyi, J. Modified Titanium Dioxide for Photocatalytic Applications. In *Photocatalysts - Applications and Attributes*; Bahadar Khan, S., Akhtar, K., Eds.; IntechOpen, 2019. https://doi.org/10.5772/intechopen.79374.

(28) Coy, E.; Siuzdak, K.; Pavlenko, M.; Załęski, K.; Graniel, O.; Ziółek, M.; Balme, S.; Miele, P.; Weber, M.; Bechelany, M.; Iatsunskyi, I. Enhancing Photocatalytic Performance and Solar Absorption by Schottky Nanodiodes Heterojunctions in Mechanically Resilient Palladium Coated TiO2/Si Nanopillars by Atomic Layer Deposition. *Chem. Eng. J.* **2020**, *392*, 123702. https://doi.org/10.1016/j.cej.2019.123702.

(29) Asahi, R.; Morikawa, T.; Ohwaki, T.; Aoki, K.; Taga, Y. Visible-Light Photocatalysis in Nitrogen-Doped Titanium Oxides. *Science* **2001**, *293* (5528), 269–271. https://doi.org/10.1126/science.1061051.

(30) Mills, A.; Le Hunte, S. An Overview of Semiconductor Photocatalysis. *J. Photochem. Photobiol. Chem.* **1997**, *108* (1), 1–35. https://doi.org/10.1016/S1010-6030(97)00118-4.

(31) Nasr, O.; Mohamed, O.; Al-Shirbini, A.-S.; Abdel-Wahab, A.-M. Photocatalytic Degradation of Acetaminophen over Ag, Au and Pt Loaded TiO2 Using Solar Light. *J. Photochem. Photobiol. Chem.* **2019**, *374*, 185–193. https://doi.org/10.1016/j.jphotochem.2019.01.032.

(32) Nasr, M.; Soussan, L.; Viter, R.; Eid, C.; Habchi, R.; Miele, P.; Bechelany, M. High Photodegradation and Antibacterial Activity of BN–Ag/TiO_2 Composite Nanofibers under Visible Light. *New J. Chem.* **2018**, *42* (2), 1250–1259. https://doi.org/10.1039/C7NJ03183A.

(33) Khojasteh, H.; Salavati-Niasari, M.; Sangsefidi, F. S. Photocatalytic Evaluation of RGO/TiO2NWs/Pd-Ag Nanocomposite as an Improved Catalyst for Efficient Dye Degradation. *J. Alloys Compd.* **2018**, *746*, 611–618. https://doi.org/10.1016/j.jallcom.2018.02.345.

(34) Zhu, Y.; Gao, C.; Bai, S.; Chen, S.; Long, R.; Song, L.; Li, Z.; Xiong, Y. Hydriding Pd Cocatalysts: An Approach to Giant Enhancement on Photocatalytic CO2 Reduction into CH4. *Nano Res.* **2017**, *10* (10), 3396–3406. https://doi.org/10.1007/s12274-017-1552-0.

(35) Jiang, L.; Huang, Y.; Liu, T. Enhanced Visible-Light Photocatalytic Performance of Electrospun Carbon-Doped TiO2/Halloysite Nanotube Hybrid Nanofibers. *J. Colloid Interface Sci.* **2015**, *439*, 62–68. https://doi.org/10.1016/j.jcis.2014.10.026.

(36) Meng, A.; Zhang, L.; Cheng, B.; Yu, J. TiO_2–MnO_x–Pt Hybrid Multiheterojunction Film Photocatalyst with Enhanced Photocatalytic CO_2-Reduction Activity. *ACS Appl. Mater. Interfaces* **2019**, *11* (6), 5581–5589. https://doi.org/10.1021/acsami.8b02552.

(37) Nasr, M.; Viter, R.; Eid, C.; Habchi, R.; Miele, P.; Bechelany, M. Enhanced Photocatalytic Performance of Novel Electrospun BN/TiO_2 Composite Nanofibers. *New J. Chem.* **2017**, *41* (1), 81–89. https://doi.org/10.1039/C6NJ03088B.

(38) Lee, C.-G.; Na, K.-H.; Kim, W.-T.; Park, D.-C.; Yang, W.-H.; Choi, W.-Y. TiO2/ZnO Nanofibers Prepared by Electrospinning and Their Photocatalytic Degradation of Methylene Blue Compared with TiO2 Nanofibers. *Appl. Sci.* **2019**, *9* (16), 3404. https://doi.org/10.3390/app9163404.

(39) Sayegh, S.; Tanos, F.; Nada, A.; Lesage, G.; Zaviska, F.; Petit, E.; rouessac, vincent; yatsunskiy, igor; Coy, E.; Viter, R.; damberga, daina; Weber, M.; Razzouk, A.; Stephan, J.; Bechelany, M. Tunable TiO2-BN-Pd Nanofibers by Combining Electrospinning and Atomic Layer Deposition to Enhance Photodegradation of Acetaminophen. *Dalton Trans.* **2022**, 10.1039.D1DT03715C. https://doi.org/10.1039/D1DT03715C.

(40) Park, S.-M.; Razzaq, A.; Park, Y. H.; Sorcar, S.; Park, Y.; Grimes, C. A.; In, S.-I. Hybrid Cu_xO–TiO_2 Heterostructured Composites for Photocatalytic CO_2 Reduction into Methane Using Solar Irradiation: Sunlight into Fuel. *ACS Omega* **2016**, *1* (5), 868–875. https://doi.org/10.1021/acsomega.6b00164.

(41) Tang, C.; Li, J.; Bando, Y.; Zhi, C.; Golberg, D. Improved TiO2 Photocatalytic Reduction by the Intrinsic Electrostatic Potential of BN Nanotubes. *Chem. - Asian J.* **2010**, *5* (5), 1220–1224. https://doi.org/10.1002/asia.200900613.

(42) Fu, X.; Hu, Y.; Yang, Y.; Liu, W.; Chen, S. Ball Milled H-BN: An Efficient Holes Transfer Promoter to Enhance the Photocatalytic Performance of TiO2. *J. Hazard. Mater.* **2013**, *244–245*, 102–110. https://doi.org/10.1016/j.jhazmat.2012.11.033.

(43) Lin, L.; Jiang, W.; Bechelany, M.; Nasr, M.; Jarvis, J.; Schaub, T.; Sapkota, R. R.; Miele, P.; Wang, H.; Xu, P. Adsorption and Photocatalytic Oxidation of Ibuprofen Using Nanocomposites of TiO2 Nanofibers Combined with BN Nanosheets: Degradation Products and Mechanisms. *Chemosphere* **2019**, *220*, 921–929. https://doi.org/10.1016/j.chemosphere.2018.12.184.

(44) Abid, M.; Sayegh, S.; Iatsunskyi, I.; Coy, E.; Lesage, G.; Ramanavicius, A.; Ben Haj Amara, A.; Bechelany, M. Design of Halloysite-Based Nanocomposites by Electrospinning for Water Treatment. *Colloids Surf. Physicochem. Eng. Asp.* **2022**, *651*, 129696. https://doi.org/10.1016/j.colsurfa.2022.129696.

(45) Biscarat, J.; Bechelany, M.; Pochat-Bohatier, C.; Miele, P. Graphene-like BN/Gelatin Nanobiocomposites for Gas Barrier Applications. *Nanoscale* **2015**, *7* (2), 613–618. https://doi.org/10.1039/C4NR05268D.

(46) Thangaraj, V.; Bussiere, J.; Janot, J.; Bechelany, M.; Jaber, M.; Subramanian, S.; Miele, P.; Balme, S. Fluorescence Quenching of Sulfo-rhodamine Dye over Graphene Oxide and Boron Nitride Nanosheets. *Eur. J. Inorg. Chem.* **2016**, *2016* (13–14), 2125–2130. https://doi.org/10.1002/ejic.201501153.

(47) Kawrani, S.; Nada, A. A.; Bekheet, M. F.; Boulos, M.; Viter, R.; Roualdes, S.; Miele, P.; Cornu, D.; Bechelany, M. Enhancement of Calcium Copper Titanium Oxide Photoelectrochemical Performance Using Boron Nitride Nanosheets. *Chem. Eng. J.* **2020**, *389*, 124326. https://doi.org/10.1016/j.cej.2020.124326.

(48) Martins, P.; Kappert, S.; Nga Le, H.; Sebastian, V.; Kühn, K.; Alves, M.; Pereira, L.; Cuniberti, G.; Melle-Franco, M.; Lanceros-Méndez, S. Enhanced Photocatalytic Activity of Au/TiO2 Nanoparticles against Ciprofloxacin. *Catalysts* **2020**, *10* (2), 234. https://doi.org/10.3390/catal10020234.

(49) Konstantinou, I. Photocatalytic Transformation of Pesticides in Aqueous Titanium Dioxide Suspensions Using Artificial and Solar Light: Intermediates and Degradation Pathways. *Appl. Catal. B Environ.* **2003**, *42* (4), 319–335. https://doi.org/10.1016/S0926-3373(02)00266-7.

(50) Mishra, G.; Mukhopadhyay, M. TiO2 Decorated Functionalized Halloysite Nanotubes (TiO2@HNTs) and Photocatalytic PVC Membranes Synthesis, Characterization and Its Application in Water Treatment. *Sci. Rep.* **2019**, *9* (1), 4345. https://doi.org/10.1038/s41598-019-40775-4.

(51) Bumajdad, A.; Madkour, M.; Abdel-Moneam, Y.; El-Kemary, M. Nanostructured Mesoporous Au/TiO2 for Photocatalytic Degradation of a Textile Dye: The Effect of Size Similarity of the Deposited Au with That of TiO2 Pores. *J. Mater. Sci.* **2014**, *49* (4), 1743–1754. https://doi.org/10.1007/s10853-013-7861-0.

(52) Addamo, M.; Bellardita, M.; Di Paola, A.; Palmisano, L. Preparation and Photoactivity of Nanostructured Anatase, Rutile and Brookite TiO2 Thin Films. *Chem. Commun.* **2006**, No. 47, 4943. https://doi.org/10.1039/b612172a.

(53) Nasr, M.; Abou Chaaya, A.; Abboud, N.; Bechelany, M.; Viter, R.; Eid, C.; Khoury, A.; Miele, P. Photoluminescence: A Very Sensitive Tool to Detect the Presence of Anatase in Rutile Phase Electrospun TiO 2 Nanofibers. *Superlattices Microstruct.* **2015**, *77*, 18–24. https://doi.org/10.1016/j.spmi.2014.10.034.

(54) Nalbandian, M. J.; Zhang, M.; Sanchez, J.; Kim, S.; Choa, Y.-H.; Cwiertny, D. M.; Myung, N. V. Synthesis and Optimization of Ag–TiO2 Composite Nanofibers for Photocatalytic Treatment of Impaired Water Sources. *J. Hazard. Mater.* **2015**, *299*, 141–148. https://doi.org/10.1016/j.jhazmat.2015.05.053.

(55) Zhao, Y.; Liu, Z.; Cao, C.; Wang, C.; Fang, Y.; Huang, Y.; Yu, C.; Zhang, J.; Li, L.; Hu, L.; Tang, C. Self-Sacrificed Template Synthesis of Ribbon-like Hexagonal Boron Nitride Nano-Architectures and Their Improvement on Mechanical and Thermal Properties of PHA Polymer. *Sci. Rep.* **2017**, *7* (1), 9006. https://doi.org/10.1038/s41598-017-08524-7.

(56) Wu, D.; Guo, J.; Wang, H.; Zhang, X.; Yang, Y.; Yang, C.; Gao, Z.; Wang, Z.; Jiang, K. Green Synthesis of Boron and Nitrogen Co-Doped TiO2 with Rich B-N Motifs as Lewis Acid-Base Couples for the Effective Artificial CO2 Photoreduction under Simulated Sunlight. *J. Colloid Interface Sci.* **2021**, *585*, 95–107. https://doi.org/10.1016/j.jcis.2020.11.075.

(57) de Jesus Gaffney, V.; Almeida, C. M. M.; Rodrigues, A.; Ferreira, E.; Benoliel, M. J.; Cardoso, V. V. Occurrence of Pharmaceuticals in a Water Supply System and Related Human Health Risk Assessment. *Water Res.* **2015**, *72*, 199–208. https://doi.org/10.1016/j.watres.2014.10.027.

(58) Palmer, P. M.; Wilson, L. R.; O'Keefe, P.; Sheridan, R.; King, T.; Chen, C.-Y. Sources of Pharmaceutical Pollution in the New York City Watershed. *Sci. Total Environ.* **2008**, *394* (1), 90–102. https://doi.org/10.1016/j.scitotenv.2008.01.011.

(59) Alalm, M. G.; Tawfik, A.; Ookawara, S. Degradation of Four Pharmaceuticals by Solar Photo-Fenton Process: Kinetics and Costs Estimation. *J. Environ. Chem. Eng.* **2015**, *3* (1), 46–51. https://doi.org/10.1016/j.jece.2014.12.009.

(60) Pacheco-Álvarez, M.; Picos Benítez, R.; Rodríguez-Narváez, O. M.; Brillas, E.; Peralta-Hernández, J. M. A Critical Review on Paracetamol Removal from Different Aqueous Matrices by Fenton and Fenton-Based Processes, and Their Combined Methods. *Chemosphere* **2022**, *303*, 134883. https://doi.org/10.1016/j.chemosphere.2022.134883.

(61) Štengl, V.; Henych, J.; Slušná, M. H-BN-TiO $_2$ Nanocomposite for Photocatalytic Applications. *J. Nanomater.* **2016**, *2016*, 1–12. https://doi.org/10.1155/2016/4580516.

(62) Ide, Y.; Liu, F.; Zhang, J.; Kawamoto, N.; Komaguchi, K.; Bando, Y.; Golberg, D. Hybridization of Au Nanoparticle-Loaded TiO2 with BN Nanosheets for Efficient Solar-Driven Photocatalysis. *J. Mater. Chem. A* **2014**, *2* (12), 4150. https://doi.org/10.1039/c3ta13769d.

(63) Zhu, S.; Wang, D. Photocatalysis: Basic Principles, Diverse Forms of Implementations and Emerging Scientific Opportunities. *Adv. Energy Mater.* **2017**, *7* (23), 1700841. https://doi.org/10.1002/aenm.201700841.

(64) Gómez-Avilés, A.; Peñas-Garzón, M.; Bedia, J.; Rodriguez, J. J.; Belver, C. C-Modified TiO2 Using Lignin as Carbon Precursor for the Solar Photocatalytic Degradation of Acetaminophen. *Chem. Eng. J.* **2019**, *358*, 1574–1582. https://doi.org/10.1016/j.cej.2018.10.154.

(65) Fidecka, K.; Giacoboni, J.; Picconi, P.; Vago, R.; Licandro, E. Quantification of Amino Groups on Halloysite Surfaces Using the Fmoc-Method. *RSC Adv.* **2020**, *10* (24), 13944–13948. https://doi.org/10.1039/D0RA01994A.

(66) Konstantinou, I. K.; Albanis, T. A. TiO2-Assisted Photocatalytic Degradation of Azo Dyes in Aqueous Solution: Kinetic and Mechanistic Investigations. *Appl. Catal. B Environ.* **2004**, *49* (1), 1–14. https://doi.org/10.1016/j.apcatb.2003.11.010.

(67) Le, T. X. H.; Nguyen, T. V.; Amadou Yacouba, Z.; Zoungrana, L.; Avril, F.; Nguyen, D. L.; Petit, E.; Mendret, J.; Bonniol, V.; Bechelany, M.; Lacour, S.; Lesage, G.; Cretin, M. Correlation between Degradation Pathway and Toxicity of Acetaminophen and Its By-Products by Using the Electro-Fenton Process in Aqueous Media. *Chemosphere* **2017**, *172*, 1–9. https://doi.org/10.1016/j.chemosphere.2016.12.060.

(68) Singh, B.; kaur, G.; Singh, P.; Singh, K.; Sharma, J.; Kumar, M.; Bala, R.; Meena, R.; Sharma, S. K.; Kumar, A. Nanostructured BN–TiO $_2$ Composite with Ultra-High Photocatalytic Activity. *New J. Chem.* **2017**, *41* (20), 11640–11646. https://doi.org/10.1039/C7NJ02509B.

(69) Ni, G.; Li, Y.; Wang, S.; Li, Q. Construction of 1D/2D BN/TiO2 Nanostructures for Efficient Photocatalytic Degradation of Dyes. *Mater. Lett.* **2021**, *288*, 129385. https://doi.org/10.1016/j.matlet.2021.129385.

(70) Li, Q.; Hou, X.; Fang, Z.; Yang, T.; Chen, J.; Cui, X.; Liang, T.; Shi, J. Construction of Layered H-BN/TiO2 Hetero-Structure and Probing of the Synergetic Photocatalytic Effect. *Sci. China Mater.* **2020**, *63* (2), 276–287. https://doi.org/10.1007/s40843-019-1180-8.

(71) Lin, L.; Jiang, W.; Nasr, M.; Bechelany, M.; Miele, P.; Wang, H.; Xu, P. Enhanced Visible Light Photocatalysis by TiO_2 –BN Enabled Electrospinning of Nanofibers for Pharmaceutical Degradation and Wastewater Treatment. *Photochem. Photobiol. Sci.* **2019**, *18* (12), 2921–2930. https://doi.org/10.1039/C9PP00304E.